Wind retrieval from RADARSAT SAR images:

Selection of a suitable C-band HH polarization wind retrieval model[1]

Paris W. Vachon

Canada Centre for Remote Sensing
588 Booth St., Ottawa, Ont. K1A 0Y7 Canada
Phone: 613 995-1575
Fax: 613 947-1385
E-mail: paris.vachon@ccrs.nrcan.gc.ca

Fred W. Dobson

Fisheries and Oceans Canada
Bedford Institute of Oceanography
Dartmouth, N.S. B2Y 4A2 Canada
Phone: 902 426-3584
Fax: 902 426-7827/2256
E-mail: DobsonF@mar.DFO-MPO.gc.ca

22 October 1999

Summary – *A standardized analysis of wind retrieval collocations from a set of ERS (C-band VV polarization) and RADARSAT (C-band HH polarization) synthetic aperture radar (SAR) open ocean images is presented. The field validation opportunities, carried out over the past eight years, provided collocated (in time and space)* in situ *validation data consisting of wind vector and ocean wave spectrum measurements. In this paper, we present validation results for the SAR-estimated wind direction and speed. The direction estimate is based on the orientation of coherent atmospheric structures in the SAR image. The speed estimate is based on a scatterometer wind retrieval model for C-band VV polarization (specifically, CMOD_IFR2) modified for HH polarization using available polarization ratios. We consider several C-band polarization ratios including empirical and theoretical forms. Use of CMOD_IFR2 and a polarization ratio according to Kirchhoff is recommended for RADARSAT SAR ocean wind retrieval.*

[1] To appear, *Canadian Journal of Remote Sensing*, ADRO Special Issue.

1. Introduction

Wind information estimated from SAR ocean images is becoming of increasing interest; several possible roles for SAR-derived wind speeds have been proposed. For example, the SAR-derived wind speed could be used as additional information to aid the interpretation of SAR images acquired for other purposes such as ship detection, oil slick detection, or search and rescue operations. Second, SAR-derived winds may be used to improve site-specific weather forecasting in regions that are too small for relatively large (25 km to 50 km) scatterometer resolution cells, such as in the coastal or marginal ice zones, or in lakes or estuaries. Third, SAR images could be used as an approach to near-shore wind climatology over small spatial scales, information that could be used for coastal windmill placement, for example. Fourth, SAR-derived winds could be assimilated into coupled atmosphere-ocean models (possibly along with SAR-derived spectral ocean wave information). And fifth, SAR ocean images could be used to study atmospheric processes at the ocean surface such as atmospheric gravity waves, wakes, hurricanes, cold air outbreaks, and polar lows.

There are two main approaches to estimating wind speed from SAR ocean images. In the first approach, the wind speed is estimated from the measured normalized radar cross section σ^o knowing the wind direction and the SAR geometry [Scoon *et al*., 1996; Vachon and Dobson, 1996; Wackerman *et al*., 1996; Fetterer *et al.*, 1998; Korsbakken *et al.*, 1998; Lehner *et al.*, 1998]. This requires good SAR image absolute radiometric calibration and a wind retrieval model function that relates the ocean wind speed to the normalized radar cross section, the relative wind direction, and the local incidence angle. Such models have been developed for ocean wind scatterometry. For SAR, the wind direction may be estimated by measuring the orientation of low frequency coherent structures in the SAR image. In the second approach, the wind speed is estimated from the degree of azimuth cut-off of the SAR image spectrum [Vachon *et al*., 1994; Kerbaol *et al*., 1998]. This procedure requires a robust measurement of the spectral width as well as a model describing the relationship between the cut-off wavelength, the wind

speed, and the ocean wave spectrum. In this paper, we focus only on the normalized radar cross section method.

For the C-band VV polarization ERS SARs, there are several well-developed wind retrieval models to draw on. We have relied on the empirically derived CMOD_IFR2 [IFREMER-CERSAT, 1996], which is used for post processing of ERS Scatterometer data. For the C-band HH polarization RADARSAT SAR, similarly well-developed and validated wind retrieval models do not exist. Our approach has been to use a hybrid model that is composed of CMOD_IFR2 and a suitable C-band polarization ratio [Vachon *et al.*, 1997a]. We will consider the performance of this class of hybrid model for RADARSAT SAR wind retrieval based on several available polarization ratios. Some of these polarization ratios are empirical in origin while others are theoretical.

In this paper, we first review the SAR image and validation data sets we have acquired along with the processing methodology. We then present the validation results for ERS and RADARSAT, and consider several possible C-band polarization ratios.

2. Data Sets

We have considered three satellite SAR sensors, as summarized in Table 1. Collocations between SAR images from these sensors and *in situ* measurements of wind and waves were obtained from a number of field programs and acquisition activities carried out over the past eight years, as summarized in Table 2. For most of our cases, the *in situ* measurement point lies within the SAR image and the *in situ* data were being measured and recorded at the time of the SAR pass (*i.e.*, exact collocations). Our first validation work was in the context of a dedicated ERS-1 calibration and validation (ERS-1 Cal/Val) voyage of CSS *Hudson* to the Grand Banks in 1991 [Dobson and Vachon, 1994]. Subsequent ERS SAR validation opportunities included the Canadian Atlantic Storms Program (CASP) II in 1992, and the Sea Truth and Remote Sensing (STARS) experiment in 1994. Our first RADARSAT validation opportunity was during the March/April Ship Detection Experiment (MASDE) held off Halifax in 1996 [Vachon *et*

al., 1997a]. Subsequent RADARSAT SAR validation opportunities included measurements taken during the recovery of the barge *Irving Whale* in the Gulf of St. Lawrence in 1996 and during the voyage of R/V *Knorr* to the Labrador Sea in 1997 for the Labrador Sea Deep Convection Experiment.

To obtain a more significant number of collocations and in an attempt to obtain measurements at higher wind speeds, SAR images were also acquired over AES and NOAA operational buoys off the East Coast and during the Storm Wave Study (SWS) 2. The latter is our most recent field activity and included wind and wave measurements near Hibernia during the winter of 1997/98. For these latter data sets, we required that the temporal collocation constraint be relaxed from contemporaneous to less than 30 minutes between SAR and buoy measurements, since the buoys were on hourly operational measurement schedules.

3. SAR Data Processing

All of the SAR data were received at CCRS in RAW (*i.e.*, signal data) format to optimize our flexibility in data processing and calibration. For this exercise, we considered only single beam RADARSAT modes within the standard acquisition swath (thus excluding ScanSAR and extended beam modes, whose calibration is less accurate than that of the single beams). The RAW data were processed to standard format calibrated images on a workstation-based SAR processor at CCRS. For the ERS data, the images were processed to the ESA precision image (*i.e.*, PRI) standard, while for the RADARSAT data, the images were processed to the SAR georeferenced fine resolution (*i.e.*, SGF) standard with radiometric calibration consistent with that of the Canadian Data Processing Facility. In both cases, the RAW signal data were first analyzed for evidence of analogue-to-digital converter saturation, and appropriate power loss correction scaling factors were derived and applied to the calibrated images [see Vachon *et al*., 1997b].

3.1 Wind Direction

We measured the orientation of the low wavenumber image spectrum to estimate the wind direction (with a 180º direction ambiguity) [Vachon and Dobson, 1996]. This assumes that the low wavenumber energy is aligned with the wind direction, as might be the case for coherent structures such as boundary layer rolls in the atmosphere. Examples of low wavenumber image spectra from ERS-2 and RADARSAT, derived from 18 km by 18 km regions of each image centred on the *in situ* wind vector measurement location, are shown in Fig. 1.

Image signatures associated with other secondary atmospheric flow phenomena, such as atmospheric gravity waves [Vachon *et al*., 1995], also produce coherent structures that can be measured by SAR at the ocean surface. The presence of these features would result in an incorrect wind direction estimate. Gravity waves, for example, usually propagate in the direction of maximum wind shear, which is generally different from the near surface wind direction of interest.

3.2 Wind Speed

We use the measured normalized radar cross section estimated from 2 km by 2 km regions in each SAR image centred on the *in situ* wind vector measurement location, the SAR geometry, and the C-band VV polarization scatterometer wind retrieval model CMOD_IFR2 [IFREMER-CERSAT, 1996] to estimate the wind speed [see Vachon and Dobson, 1996]. In the case of RADARSAT, we use a similar approach, except that the model is modified to become a hybrid C-band HH scatterometer wind retrieval model [Vachon *et al*., 1997a] by using CMOD_IFR2 and either empirical or theoretical C-band polarization ratios. We define the polarization ratio as:

$$PR = 10 \log_{10}(\sigma^{o}_{VV}/\sigma^{o}_{HH}), \qquad [dB] \qquad (1)$$

where σ^{o}_{VV} and σ^{o}_{HH} are the VV and HH polarization normalized radar cross sections, respectively. Then, the hybrid model polarization ratio is given by

$$\sigma^o_{HH} = \text{CMOD\_IFR2}(U,\varphi,\theta) - PR, \qquad [\text{dB}] \qquad (2)$$

where U is the neutral stability wind speed at 10 m height, φ is the relative wind direction (symmetrical about 0º which corresponds to the wind blowing towards the radar), and θ is the local angle of incidence.

There are several possible choices for PR. One choice is to use the empirically measured polarization ratios that were reported by Unal *et al.* [1991]. We denote these wind speed and incidence angle dependent C-band polarization ratios, presented in Table 3, as PR^U. We have used these polarization ratios in our previous RADARSAT SAR wind retrieval efforts by interpolating within this data table [see Vachon *et al*., 1997a]. For RADARSAT incidence angles (nominally 20º to 50º), σ^o_{HH} is smaller than σ^o_{VV}, and decreases more rapidly with increasing incidence angle.

An alternate form for PR^U was suggested by Thompson *et al*. [1998] in which the wind speed dependence was ignored, and an incidence angle dependent model function was fitted to the data of Unal *et al*. [1991] at 10 ms^{-1}. The following form was proposed for the C-band polarization ratio:

$$PR^T = [(1 + 2\tan^2(\theta))/(1 + 0.6\tan^2(\theta))]^2, \qquad [\text{linear units}] \qquad (3)$$

This form is closely related to some other theoretical forms, as will be shown below.

Some theoretical polarization ratios have been summarized in the work of Elfouhaily [1997] and Elfouhaily *et al.* [1999]. From this work we can deduce the C-band polarization ratio for Bragg scattering:

$$PR^B = [(1 + 2\tan^2(\theta))/(1 + 0.0\tan^2(\theta))]^2, \qquad [\text{linear units}] \qquad (4)$$

(the null coefficient is included in the denominator to illustrate the relationship to equation (3) and other theoretical polarization ratio forms). For Kirchhoff scattering:

$$PR^K = [(1 + 2\tan^2(\theta))/(1 + 1.0\tan^2(\theta))]^2. \qquad [\text{linear units}] \qquad (5)$$

Based on the extended scattering model of Elfouhaily:

$$PR^E = [(1 + 2\tan^2(\theta))/(1 + 2\sin^2(\theta))]^2. \qquad \text{[linear units]} \qquad (6)$$

Each of these polarization ratio forms is plotted in Fig. 6, which will be considered below.

It should be noted that an error in wind direction could cause an error in the estimated wind speed. The minimum (upwind look direction) and maximum (cross wind look direction) wind speeds for an observed value of σ^o (*i.e.*, if the wind direction is not known) for two different incidence angles and our hybrid HH model based on PR^U, are shown in Fig. 2. Also shown are the maximum wind speed errors for a given error in wind direction. For example, for an error in wind direction of $\delta\varphi = 30^o$ at an incidence angle of $\theta = 23^o$, and for a true upwind wind speed of 10 ms^{-1}, the estimated wind speed could be in error by more than 5 ms^{-1}.

Example comparisons between observed and modelled σ^o profiles for ERS-1 (versus CMOD_IFR2) and RADARSAT (versus the hybrid model with PR^U) are shown in Fig. 3. The model curves are based on the *in situ* measured wind vector. As noted previously, all of the SAR data have been corrected for ADC saturation power loss. Both the corrected and uncorrected profiles are shown for the ERS-1 case; ADC saturation power loss correction was not required for the RADARSAT data in these examples. The *in situ* wind measurement was taken at the location of the vertical solid line. The agreement between the observed σ^o profiles and the model curves is seen to be excellent in terms of the overall signal level and the profile slope.

4. Validation Results

Not all images acquired were suitable for wind retrieval validation. Data points were rejected for cases of low wind speed ($U < 2$ ms^{-1}) and poor signal-to-noise ratio (SNR < 5 dB). Data were also rejected if there was evidence of mesoscale variability within the scene (for example, if an atmospheric front was near the buoy location). We imposed this restriction since we are relating a spatial average

from the SAR image to a temporal average from the *in situ* sensor, requiring local homogeneity in space and time for a meaningful comparison. Based on these criteria, 115 observations out of the 142 in our initial database were retained for subsequent analysis.

4.1 Wind Direction

The histogram of the difference between the *in situ* measured wind direction and the SAR-derived wind direction, after resolving the 180º wind direction ambiguity, for both ERS and RADARSAT cases is shown in Fig. 4. The horizontal dashed line represents a uniform distribution of directional differences, which would apply if the SAR-derived wind directions were completely random. The uniform distribution has a standard deviation of 52º. The RMS error for the SAR-derived wind direction is about 40º. We have found that the SAR-derived direction is within 30º of the *in situ* measurement for about half of the cases we have worked with. In general, the SAR-derived wind direction is best under higher wind and unstable atmospheric conditions (*i.e.*, when the water temperature exceeds the air temperature, resulting in convection and the possible formation of atmospheric boundary layer rolls) and the rolls are readily visible in the SAR image.

4.2 Wind Speed

As mentioned previously, to date, we have been using a hybrid C-band HH polarization model based on PR^U for our RADARSAT SAR wind retrieval. In Fig. 5, we present a regression of the SAR-derived wind speeds under the assumption that the wind direction is known (in this case, represented by the *in situ* wind direction measurement) versus the *in situ* measured wind speed. For this plot and subsequent regressions, rms1 is the RMS error with respect to the best-fit line through the data, while rms2 is the standard deviation of the difference between the two measurements. Based on the 115 observations from both SARs, the wind speed is estimated to within a RMS error of 2.7 ms^{-1} if the wind direction is known. However, the RMS error is 1.9 ms^{-1} for the 56 ERS observations and 2.9 ms^{-1} for the 59 RADARSAT observations.

The RMS error we achieved with the ERS data is essentially consistent with the wind speed retrieval performance of CMOD_IFR2 when applied to ERS scatterometer data. It is evident that the RADARSAT wind speeds are overestimated, especially at higher wind speeds, suggesting inadequacies in the use of PR^U in our hybrid model. Specifically, PR^U appears to be too large.

In order to address potential problems with PR^U, we have estimated C-band polarization ratios from the RADARSAT observations and CMOD_IFR2 as

$$PR = CMOD\_IFR2(U,\varphi,\theta) - \sigma^o_{R'SAT}, \quad [dB] \qquad (7)$$

which have been plotted in Fig. 6 as a function of incidence angle along with a best fit line through these polarization ratios, PR^U for 10 ms^{-1}, and the theoretical polarization ratio forms of equations (3) through (6). From this plot, we note the following:

- The estimated values of PR have considerable scatter, indicating that their dependence on incidence angle is too simplistic (it is likely that they should also be parameterized in terms of wind speed and wind direction, among other things);
- PR^T is indeed a reasonable fit to PR^U at 10 ms^{-1};
- PR^U is generally larger than the polarization ratios estimated from equation (7), accounting for the tendency to overestimate the retrieved wind speed from RADARSAT when used with CMOD_IFR2;
- PR^B is larger still;
- PR^K and PR^E are better fits to the polarization ratios derived from equation (7), although PR^E seems to be increasing too rapidly with larger incidence angles.

In Fig. 7 we have re-plotted the RADARSAT data of Fig. 5 based on PR^U (left) and PR^K (right). We see that use of PR^K in the hybrid C-band HH polarization model has reduced the RMS error in the

retrieved wind speed from 2.9 ms^{-1} to 2.4 ms^{-1}. Although this performance is worse than that of ERS data with CMOD_IFR2, it is significantly better than we initially achieved with PR^U, and the wind speeds retrieved from the RADARSAT data no longer appear to be overestimated. Use of PR^E, or the best fit to the observed polarization ratios, provides similar benefits and could also be recommended. However, we find it attractive to use an analytical polarization ratio and we were concerned about the growth of PR^E with increasing incidence angle.

5. Conclusions

We have considered a SAR/wind validation data set that has been compiled over the past eight years and is composed of ERS-1/2 (C-band VV polarization) and single beam RADARSAT (C-band HH polarization) SAR images of the open ocean. A total of 142 validation data points across all 3 sensors are available. We presented only some possible results from this data set as some parts of the validation data are still being compiled and processed; analysis is ongoing. The upper limit on validated wind speed is about 20 ms^{-1}.

We have affirmed the results of previous studies, and shown that the ocean surface wind vector may be estimated from C-band VV polarization ERS SAR images using the CMOD_IFR2 scatterometer wind model. However, we have also extended this result to include C-band HH polarization RADARSAT SAR images by using a hybrid model composed of CMOD_IFR2 and a C-band polarization ratio.

The retrieved wind direction is based on the orientation of kilometer-scale coherent structures in the SAR image. The estimated direction has a 180º ambiguity. A useful SAR-derived direction (to within 30º of that measured *in situ*) is retrieved for about one-half of the cases we have considered. The directional ambiguity may be resolved using other wind effects in the SAR image (such as nearshore wind shadows), *in situ* observations, or synoptic surface analysis charts.

For ERS SAR data, we achieved a RMS wind speed error of 1.9 ms^{-1}. For RADARSAT SAR data, the wind retrieval performance is dependent upon the polarization ratio that is used in the hybrid model. For the data of Unal *et al.* [1991], we achieved a RMS wind speed error of 2.9 ms^{-1}, and noted that the SAR-derived wind speeds are overestimated at higher wind speeds. However, by using a polarization ratio based on Kirchhoff scattering, we achieved a RMS wind speed error of 2.4 ms^{-1} and eliminated the overestimation at higher wind speeds.

Based on these results, and in the absence of a validated physical model or adequate data to properly tune a C-band HH polarization empirical model, we recommend that a hybrid C-band HH polarization model be used for RADARSAT SAR wind speed retrieval. The hybrid model should use CMOD_IFR2 and a polarization ratio based on Kirchhoff scattering.

Satlantic Inc. has been developing an Ocean Monitoring Workstation (OMW) for the operational analysis of RADARSAT SAR images [Henschel *et al*., 1997]. One product from their workstation is a set of derived ocean surface wind vectors. Some of the algorithms tested in this paper were provided to Satlantic Inc. for inclusion in the OMW. Therefore, the wind vector retrieval performance reported here reflects the performance of the OMW.

6. Acknowledgements

The data acquisition and processing described in this report were carried out over many years with significant contributions from many individuals, in particular John Wolfe (CCRS) and John Campbell (now of DREO). Thanks also to Harald Krogstad (UTrondheim), Tony Elfouhaily (JHU/APL), and Don Thompson (JHU/APL) for helpful discussions. Bob Keeley (DFO/MEDS) supplied the operational buoy data and funded some of the analysis. Sylvia Thomas (Noetix Research Inc.) helped prepare parts of the manuscript. The original ERS data are copyright ESA, while the original RADARSAT data are copyright CSA. The RADARSAT data were obtained through the RADARSAT

Validation Program (RVP), ADRO projects #143 (Fred Dobson, PI) and #160 (Laurence Gray, PI), and through data purchase by DFO.

7. References

Dobson, F.W., and P.W. Vachon, "The Grand Banks ERS-1 SAR wave spectra validation Experiment: Program overview and data summary", *Atmosphere-Ocean*, 32(1), 7-29, 1994.

Elfouhaily, T.M., "A consistent wind and wave model and its application to microwave remote sensing of the ocean surface", Ph.D. Thesis Dissertation, Denis Diderot University (PARIS-7), Dept. of Physics, 4 January 1997.

Elfouhaily, T., D.R. Thompson, D. Vandemark, and B. Chapron, "A new bistatic model for electromagnetic scattering from perfectly conducting random surfaces", *Waves in Random Media*, 9, 281-294, 1999.

Fetterer, F., D. Gineris, C.C. Wackerman, "Validating a scatterometer wind algorithm for ERS-1 SAR", *IEEE Trans. Geoscience Rem. Sens.*, 34(2), 1343-1352, 1998.

Henschel, M.D., R.B. Olsen, P. Hoyt, and P.W. Vachon, "The ocean monitoring workstation: Experience gained with RADARSAT", in Proc. Geomatics in the Era of RADARSAT (GER'97) 27-30 May 1997, Ottawa, Canada, Proceedings on CDROM, 1997.

IFREMER-CERSAT, Off-line wind scatterometer ERS Products: User Manual, Technical Report C2-MUT-W-01-IF, Version 2.0, IFREMER - CERSAT, BP 70, 29280 PLOUZANE, France, 1996.

Kerbaol, V., B. Chapron, and P.W. Vachon, "Analysis of ERS-1/2 SAR wave mode imagettes", *J. Geophys. Res.*, 103(C3), 7833-7846, 1998.

Korsbakken, E., J.A. Johannessen, and O.M. Johannessen, "Coastal wind field retrievals from ERS synthetic aperture radar images", *J. Geophys. Res*., 103(C4), 7857-7874, 1998.

Lehner, S., J. Horstmann, W. Koch, and W. Rosental, "Mesoscale wind measurements using recalibrated ERS SAR images", *J. Geophys. Res*., 103(C4), 7847-7856, 1998.

Scoon, A., I.S. Robinson, and P.J. Meadows, "Demonstration of an improved calibration scheme for ERS-1 SAR imagery using a scatterometer wind model", *Int. J. Rem. Sens*., 17(2), 413-418, 1996.

Thompson, D.R., T.M. Elfouhaily, and B. Chapron, "Polarization ratio for microwave backscattering from the ocean surface at low to moderate incidence angles", International Geoscience and Remote Sensing Symposium (IGARSS'98), CD-ROM Proceedings, Seattle, WA, USA, July 6-10, 1998.

Unal, C. M.H., P. Snoeij, and P.J.F. Swart, "The polarization-dependent relation between radar backscatter from the ocean surface and surface wind vector at frequencies between 1 and 18 GHz", *IEEE Trans. Geoscience Rem. Sens*., 29(4), 621-626, 1991.

Vachon, P.W., J.W.M. Campbell, C. Bjerkelund, F.W. Dobson, and M.T. Rey, "Ship detection by the RADARSAT SAR: Validation of detection model predictions", *Can. J. Rem. Sens*., 23(1), 48-59, 1997a.

Vachon, P.W., and F.W. Dobson, “Validation of wind vector retrieval from ERS-1 SAR images over the ocean”, *The Global Atmosphere and Ocean System*, 5, 177-187, 1996.

Vachon, P.W., J.A. Johannessen, and D.P. Browne, “ERS-1 SAR images of atmospheric gravity waves”, *IEEE Trans. Geoscience Rem. Sens*., 33(4), 1014-1025, 1995.

Vachon, P.W., H.E. Krogstad, and J.S. Paterson, “Airborne and spaceborne synthetic aperture radar observations of ocean waves”, *Atmosphere-Ocean*, 32(1), 83-112, 1994.

Vachon, P.W., A.L. Gray, C.E. Livingstone, and A.P. Luscombe, “Adaptive compensation of RADARSAT SAR analogue-to-digital converter saturation power loss”, Geomatics in the ERA of RADARSAT (GER’97), CD-ROM Proceedings, Ottawa, Ont., Canada, May 27-30, 1997b.

Wackerman, C.C., C.L. Rufenach, R.A. Shuchman, J.A. Johannessen, and K.L. Davidson, “Wind vector retrieval using ERS-1 synthetic aperture radar imagery”, *IEEE Trans. Geoscience Rem. Sens*., 34(6), 1343-1352, 1996.

Tables:

Table 1: ERS versus RADARSAT SARs.

	ERS-1/2	*RADARSAT*
Agency	ESA	CSA
Launched	Jul'91/Apr'95	Nov'95
Sensors	SAR etc.	SAR
SAR modes	1	22 & ScanSAR
Descending node time	10:30 AM	6:30 AM
Frequency	C-band	C-band
Polarization	VV	HH
Gain	Fixed	Dynamic or Fixed
Analogue-to-digital converter	5-bits	4-bits
Nominal incidence angle	20º to 26º	20º to 50º
Nominal value of R/V	~ 115 s	115 s to 155 s

Table 2: Summary of validation field programs and numbers of collocations.

Program	*Location*	*Dates*	*ERS-1*	*ERS-2*	*R'SAT*
ERS-1 Cal/Val	Grand Banks	Nov'91	12		
CASP II	Grand Banks	Apr'92	4		
STARS'94	Grand Banks	Dec'94	1	1	
Operational Buoys	East Coast	Nov'95 – Jun'97		25	25
MASDE	Off Halifax	Mar – Apr'96	3	3	9
Irving Whale	Gulf St. Lawrence	Jul – Aug'96			3
R/V Knorr	Labrador Sea	Feb – Mar'97			6
SWS II	Hibernia	Nov'97 – Mar'98		16	34
Total			20	45	77

Table 3: C-band polarization ratios of Unal *et al.* [1991] (*i.e.*, PR^U).

θ	*2 ms^{-1}*	*4 ms^{-1}*	*6 ms^{-1}*	*8 ms^{-1}*	*10 ms^{-1}*	*12 ms^{-1}*	*14 ms^{-1}*
20º	1.05	0.79	0.65	0.56	0.51	0.49	0.49
30º	2.07	2.37	2.57	2.70	2.70	2.88	2.95
45º	4.78	5.25	5.47	5.59	5.59	5.71	5.75

List of Figures:

Figure 1: Low wavenumber image spectra from ERS-2 (left) and RADARSAT (right). The SAR-derived wind direction (dashed line) and the *in situ* measured wind direction (large arrow) are as indicated.

Figure 2: Minimum and maximum wind speeds and wind speed errors for hybrid HH model using PR^U for $\theta = 23^o$ (left) and $\theta = 43^o$ (right).

Figure 3: Examples of measured and modelled σ^o profiles for ERS-2 (left) and RADARSAT (right). ADC saturation power loss correction was not required for the RADARSAT data. The RADARSAT σ^o profile is flat over land to the left, and rises over a nadir ambiguity to the right.

Figure 4: SAR-derived wind direction histogram showing the distribution of the difference between the SAR-derived wind direction (direction ambiguity removed) and the *in situ* measured wind direction. The horizontal dashed line represents a uniform distribution of relative wind directions.

Figure 5: Regression of the SAR-derived wind speed (using *in situ* measured wind direction) versus the *in situ* measured wind speed for ERS (using CMOD_IFR2) and RADARSAT (using hybrid C-band HH model with PR^U). The dashed line is the best fit while the solid line represents a perfect fit.

Figure 6: C-band polarization ratios for various models using σ^o from RADARSAT observations and CMOD_IFR2 driven by the *in situ* wind vector.

Figure 7: Regression of measured versus RADARSAT SAR-derived wind speed (using the *in situ* measured wind direction) for hybrid C-band HH models using PR^U (left) and PR^K (right).

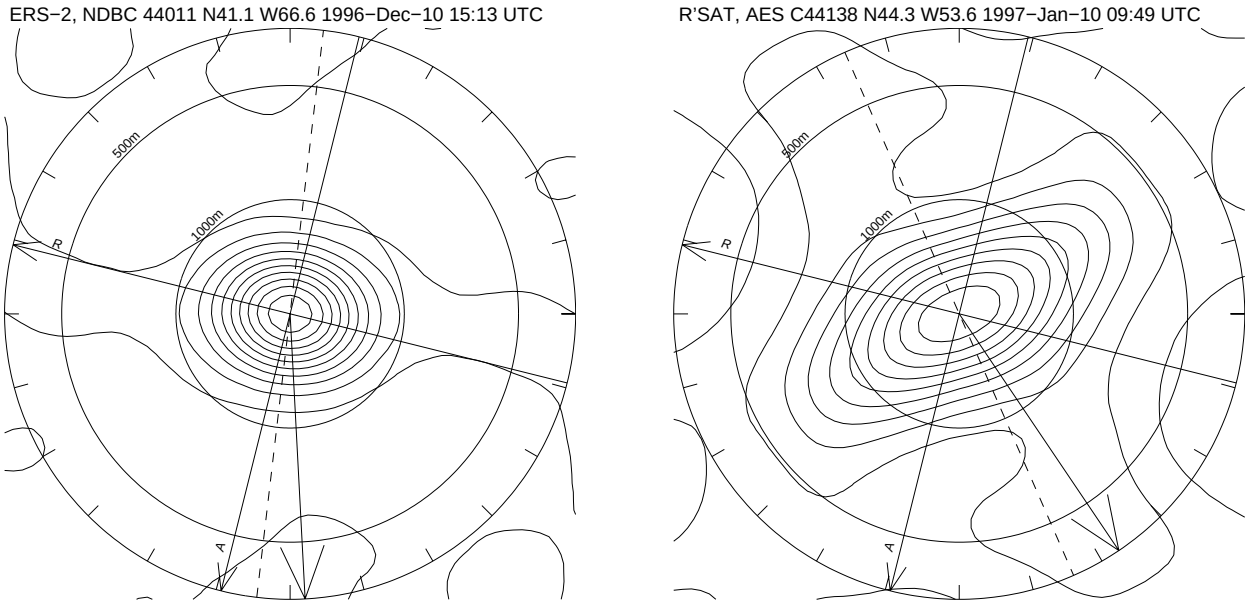

Figure 1

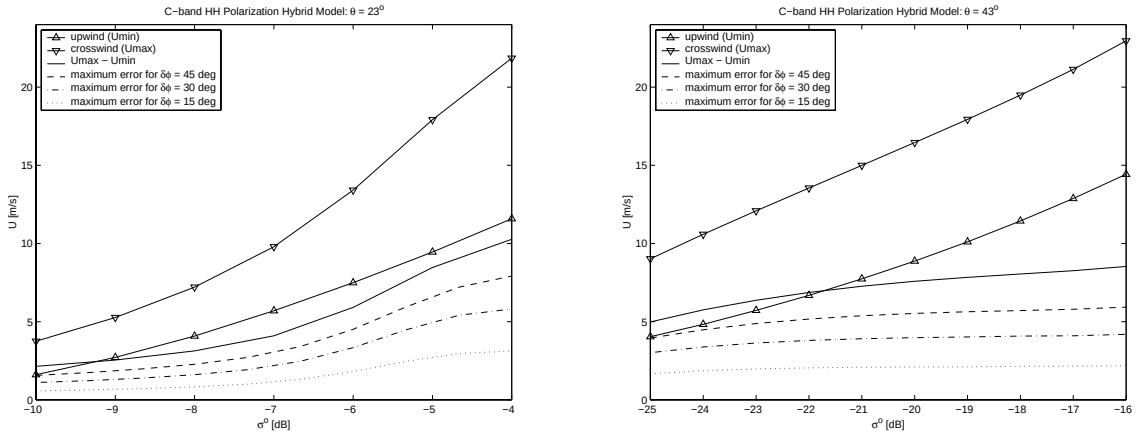

Figure 2

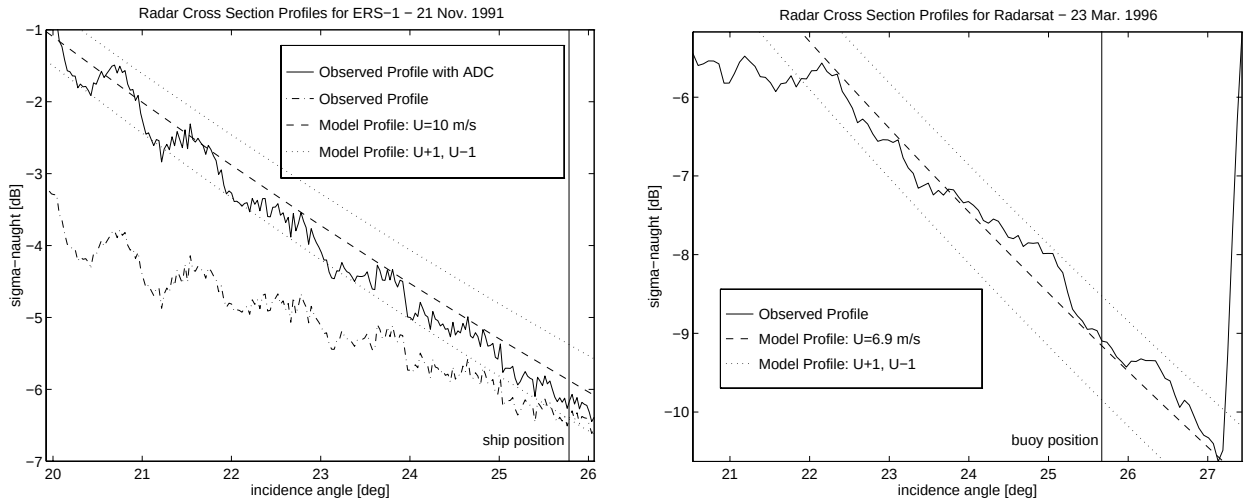

Figure 3

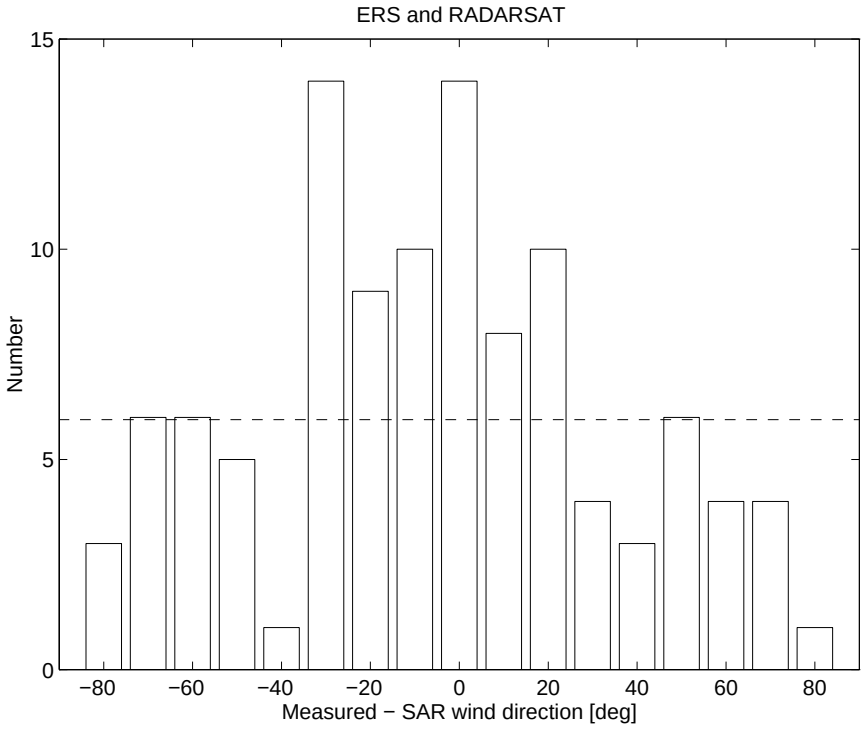

Figure 4

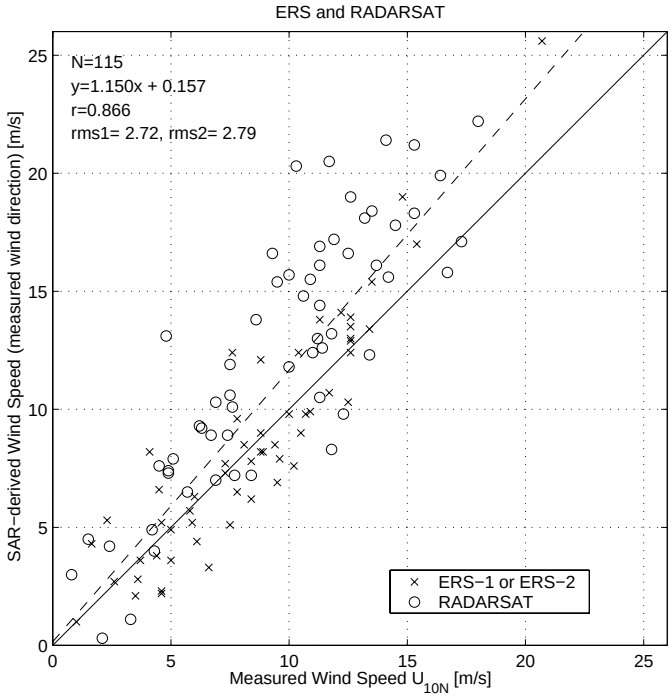

Figure 5

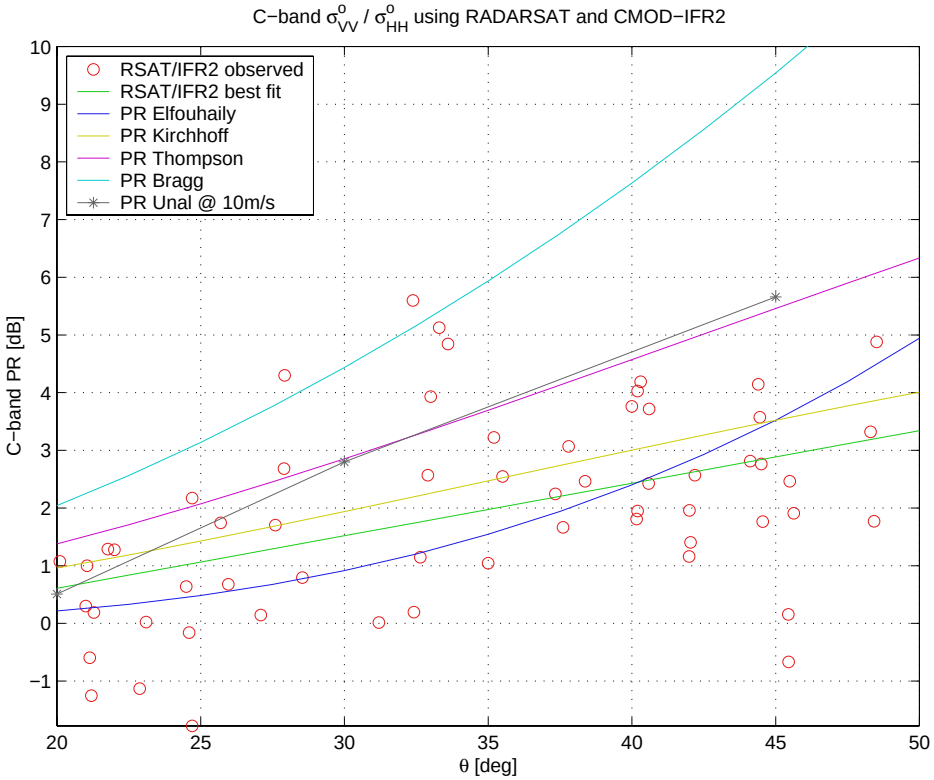

Figure 6

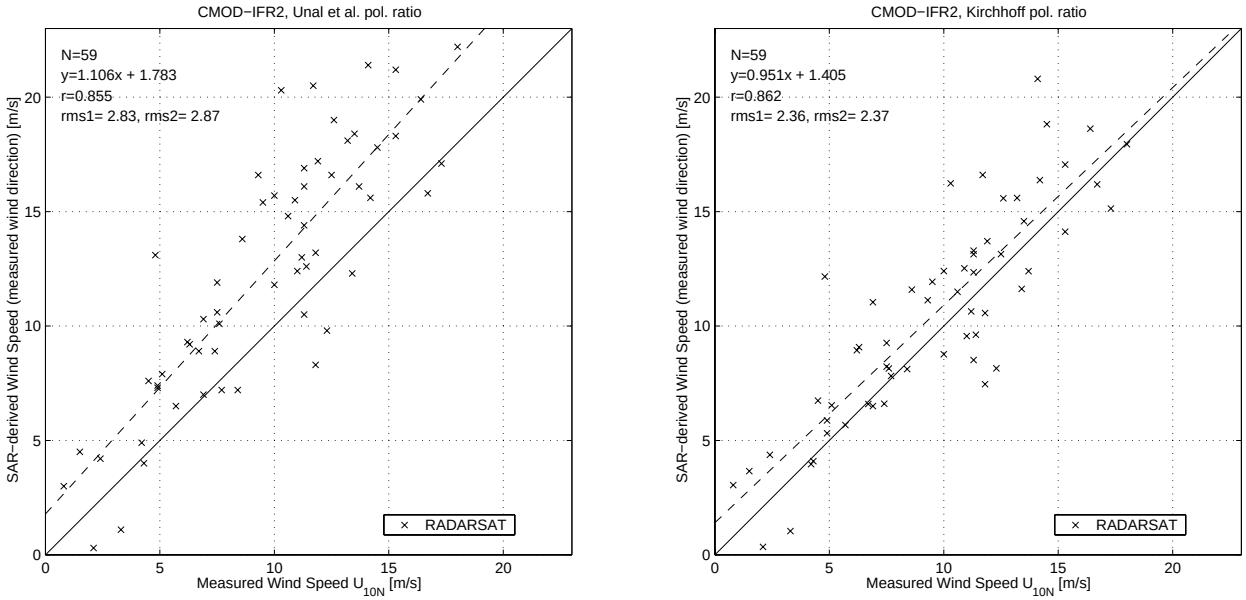
CMOD−IFR2, Unal et al. pol. ratio
N=59
y=1.106x + 1.783
r=0.855
rms1= 2.83, rms2= 2.87
RADARSAT
SAR−derived Wind Speed (measured wind direction) [m/s]
Measured Wind Speed U10N [m/s]
CMOD−IFR2, Kirchhoff pol. ratio
N=59
y=0.951x + 1.405
r=0.862
rms1= 2.36, rms2= 2.37
RADARSAT
SAR−derived Wind Speed (measured wind direction) [m/s]
Measured Wind Speed U10N [m/s]

Figure 7